Environmental Science and Pollution Research (2019) 26:4618–4632
https://doi.org/10.1007/s11356-018-3872-3

RESEARCH ARTICLE

Calcium ion incorporated hydrous iron(III) oxide: synthesis, characterization, and property exploitation towards water remediation from arsenite and fluoride

Abir Ghosh[1,2] · Suparna Paul[4,5] · Sayan Bhattacharya[3] · Palani Sasikumar[2] · Krishna Biswas[1] · Uday Chand Ghosh[2]

Received: 17 September 2018 / Accepted: 27 November 2018 / Published online: 17 December 2018

Abstract

Calcium ion-incorporated hydrous iron(III) oxide (CIHIO) samples have been prepared aiming investigation of efficiency enhancement on arsenic and fluoride adsorption of hydrous iron(III) oxide (HIO). Characterization of the optimized product with various analytical tools confirms that CIHIO is microcrystalline and mesoporous (pore width, 26.97 Å; pore diameter, 27.742 Å with pore volume 0.18 $cm^3\ g^{-1}$) material. Increase of the BET surface area (> 60%) of CIHIO (269.61 $m^2\ g^{-1}$) relative to HIO (165.6 $m^2\ g^{-1}$) is noticeable. CIHIO particles are estimated to be ~ 50 nm from AFM and TEM analyses. Although the pH optimized for arsenite and fluoride adsorptions are different, the efficiencies of CIHIO towards their adsorption are very good at pH 6.5 (pH_{zpc}). The adsorption kinetics and equilibrium data of either tested species agree well, respectively, with pseudo-second order model and Langmuir monolayer adsorption phenomenon. Langmuir capacities (mg g^{-1}at 303 K) estimated are 29.07 and 25.57, respectively, for arsenite and fluoride. The spontaneity of adsorption reactions (ΔG^0 = − 18.02 to − 20.12 kJ mol^{-1} for arsenite; − 0.2523 to − 3.352 kJ mol^{-1} for fluoride) are the consequence of entropy parameter. The phosphate ion (1 mM) compared to others influenced adversely the arsenite and/or fluoride adsorption reactions. CIHIO (2.0 g L^{-1}) is capable to abstract arsenite or fluoride above 90% from their solution (0 to 5.0 mg L^{-1}). Mechanism assessment revealed that the adsorption of arsenite occurs via chelation, while of fluoride occurs with ion-exchange.

Keywords Adsorption · Arsenite · Ca^{2+}-incorporated ferric oxide · Characterization · Fluoride

Responsible editor: Tito Roberto Cadaval Jr

Electronic supplementary material The online version of this article (https://doi.org/10.1007/s11356-018-3872-3) contains supplementary material, which is available to authorized users.

✉ Krishna Biswas
kbiswas202@gmail.com

✉ Uday Chand Ghosh
ucghosh@yahoo.co.in

[1] Department of Chemistry, Maharaja Manindra Chandra College, Kolkata, India

[2] Department of Chemistry, Presidency University, 86/1 College Street, Kolkata 700073, India

[3] School of Ecology and Environmental Studies, Nalanda University, Rajgir, Bihar, India

[4] Department of Chemistry, National Institute of Technology, Durgapur, India

[5] CSIR-Central Mechanical Engineering research institute, Durgapur, India

Introduction

The constant rapid growth of population, urban civilization, and industrialization in the world has been dramatically deteriorating the global climate and natural ecosystem owing to waste generation, which contain various pollutants including heavy metal ions (Moghaddam et al.2016), toxic organic compounds, pharmaceuticals, organic and inorganic dyes, and dissolved inorganic solids (Taghavi et al. 2018a, b).

Among the inorganic pollutants, arsenic and fluoride have attracted great attention towards the secure drinking water predominantly due to two major reasons. One is their chronic deadly effects on human health caused by high intake and the other is their natural abundance in drinkable water sources. Smedley and Kinniburgh (2002) had reported the abundance of high arsenic concentration (100–5000 μg L^{-1}) in surface and groundwater in sulfide mineralization areas. Underground aquifers in south eastern Asia (India, Bangladesh, Philippines, China), South and North South

America, and part of the Europe (Romania, Hungary, Serbia, and Croatia) are also contaminated with high arsenic (> 10 μg L^{-1}) (Smedley and Kinniburgh 2002). Less mobile arsenate occurring naturally in soil reduces to more mobile and toxic arsenite by organic matters at optimum geochemical environment, which leads to the contamination of groundwater aquifers (Mohan and Pittman 2007; Wang et al. 2015). In accordance to the US Environmental Protection Agency (Wang et al. 2015), the allowance concentration limit of $arsenic_{(total)}$ for the safe drinking water is ≤ 10 μg L^{-1} (World Health Organization 2011).

Besides arsenic, presence of the fluoride at high proportions in drinkable water sources was identified in 1937 at Nellore district (Andhra Pradesh) in India (Siddiqui 1955). Fluoride intake beyond the maximum allowance level (1.5 mg L^{-1}) of international regulation (Wang et al. 2015) may effect in progressive incapacitate disorder known as fluorosis (Fallahzadeh et al. 2018; Miri et al. 2018). Many countries including India still depend upon the groundwater due to economic viability and well accessibility. But existence of the high arsenic or fluoride in groundwater makes the water unhygienic for drinking which gains paramount attention for decontamination of arsenic/fluoride from water.

Accounting the attenuation of these contagions several water purification techniques have been studied (Pendergast and Hoek 2011; Crittenden et al. 2012; Gupta et al. 2012; Ali 2012; Li et al. 2016; Saha et al. 2016). Among them, adsorption technique is unique due to ease of operation with high purification efficiency in a low expense (Babel 2003). Multiple materials as adsorbent had been examined for arsenic and fluoride removal from aqueous phases. Fe_2O_3 (Zhong et al. 2006), Fe_3O_4 (Yavuz et al. 2006; Paul et al. 2015), FeOOH (Li et al. 2011a; Wang et al. 2012), Carbon nanospheres (Li et al. 2015),TiO_2 (Zhong et al. 2008), CeO_2 (Cao et al. 2010), CuO (Yu et al. 2012), titanium lanthanum oxide-activated carbon (Jing et al. 2012), Fe_2O_3-Silica (Yang et al. 2014), AlOOH-Fe_3O_4 (Yang et al. 2013), ZrO_2-carbon nanotubes (Addo Ntim and Mitra 2012), and Fe_3O_4-graphene (Chandra et al. 2010) were employed for the arsenic removal. The materials such as ZrO_2 (Biswas et al. 2007a), rare earth metal oxide (Raichur and Jyoti Basu 2001), manganese coated alumina (Maliyekkal et al. 2006),coal based sorbents (Sivasamy et al. 2001), fly ash (Chaturvedi et al. 1990), waste carbon slurry (Gupta et al. 2007), oxide minerals (Rongshu et al. 1995), bone char (Medellin-Castillo et al. 2007), zeolites (Mayadevi 1996), spent catalyst (Lai and Liu 1996), and activated alumina (Ku and Chiou 2002) were employed for the fluoride removal. Many of them are efficient even at high ionic concentration (Fan 2003), but some of them are expensive such as activated carbon and rare earth (Tian et al. 2011). Among them, ferric oxide was found to be cheaper as well as it has moderate affinity towards both arsenic (Zhong et al. 2006) and fluoride (Chen et al. 2012). Improved adsorption affinity of iron oxide towards arsenic and fluoride were achieved by surface modification incorporating some multivalent metal ions (Ghosh et al. 2006; Gupta et al. 2008, 2010; Chen et al. 2012). Till date very few research reports available for scavenging both arsenic and fluoride (Tian et al. 2011; Li et al. 2011a, b). Anticipated that incorporation of calcium ion inside the iron(III) oxide could be an effective cheap material for scavenging arsenite and fluoride from the aqueous phase. Hence, we report the synthetic calcium ion-incorporated hydrous iron(III) oxide (CIHIO) as a better candidate for removal of arsenite and fluoride from water. Adsorption capacity as well as mechanism has also been reported with modeling of kinetics and equilibrium data.

Materials and methods

Materials used

This section is given in Supplementary Information (SI).

Analytical tools and reagents preparation

This is given in SI section.

Experimental design

This is given in SI section.

Calcium ion-incorporated hydrous iron(III) oxide (CIHIO) preparation

Calcium ion-incorporated hydrous iron oxide (CIHIO) samples were prepared by mixing the salt solution calcium and ferric ions (mole/mole) from 0.2:1 to 1:2. NaOH solution (4 M) was dropped slowly onto the solution stirred mechanically till the supernatant pH rose up above 10.0 keeping reaction temperature 70 °C. The brown gel precipitate was separated from mother liquid after 48 h, which was washed with water till washing liquid drained out is neutral. The brown mass dried inside an oven at 80–100 °C had been treated with cold water, and re-dried at that temperature. Finally, the dried material was ground, sieved to particles size of range 52–100 mesh (149–290 μm) and, employed for arsenite and fluoride adsorption from their separate aqueous solutions. It is found that the material showed the increase of arsenite and also fluoride adsorption amount with increasing the amount of calcium ion (Figure S1). However, the CIHIO sample became hygroscopic when volume proportion of the calcium solution (0.05 M) was higher than that of the ferric solution (0.05 M).

Therefore, CIHIO sample prepared from a mixture of 0.05 M ferric solution and 0.05 M calcium solution (1: 1, *v*/*v*), which showed good arsenite/fluoride adsorption capacity, was characterized and used systematically for conducting adsorption experiments.

Arsenic and fluoride samples analysis

The methods used for analysis of arsenic and fluoride samples are given inside SI section in details.

Adsorption capacity calculation

Adsorption capacity (q, mg g^{-1}) had been calculated by the mass balanced equation (Eq. 1).

$$q = \frac{(C_i - C_f)}{m} \times \frac{V}{1000} \quad (1)$$

where C_i (mg L^{-1}) is initial concentration of solute in solution. The $q = q_t$ for C_f (mg L^{-1}) = C_t (adsorbate concentration at time, *t*; *V* = volume (mL) of the solute solution taken, m = mass (g) of CIHIO added. The $q = q_e$ for $C_f = C_e$ (adsorbate concentration at equilibrium).

Results and discussion

Characterization

Figure 1 shows SEM images (a and b), TEM image (c), EDAX spectrum for the elements over surface (d), and bar graph showing elemental percentage (e), respectively. Image a demonstrated the shape of particles while the image b showed the presence of facture in particles. The factures should be beneficial allowing penetration of solute solution inside the particles for adsorption. The TEM image c (Fig. 1) shows the presence of tiny particles inside agglomerates of size about 50 nm, which are obviously nanoparticles (NPs) in dimension. From the EDAX spectrum (d) and the elemental composition (plot e) (Fig. 1), it can be concluded that the atomic percentages (in parenthesis) of the elements over CIHIO surface are Fe (35.21), Ca (20.76), Cl (4.4), and O (39.62); indicating the atomic percentage of Ca is about 0.59 times that of Fe. Low chloride percentage found has appeared

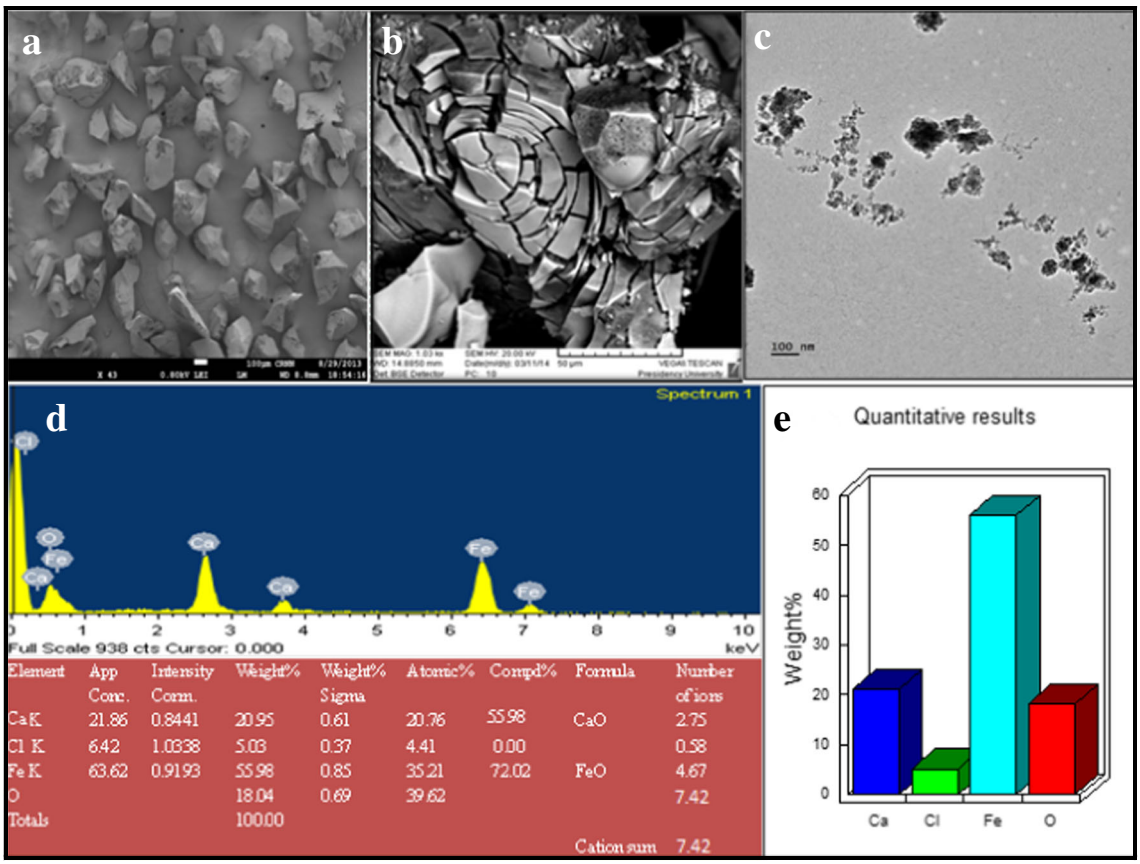

Fig. 1 The SEM mages at (**a**) low resolution and (**b**) high resolution; TEM image (**c**) (100 nm scale); (**d**) electron dispersive X-ray (EDX) spectrum with (**d**) surface elemental composition and (**e**) bar graph plots showing surface composition (**e**) of CIHIO material

from the reagents, which cannot be washed out owing to entrapping in lattice structure. Lower percentage of Ca than Fe in CIHIO is due to the higher solubility product value (K_{sp}) of calcium hydroxide (5.5×10^{-6}) than iron(III) hydroxide (4×10^{-38}). Figure 2 shows the AFM images of native hydrous ferric oxide (HFO) in 2-dimension including the particle size distribution and surface profile showing a clear smooth surface (image a). Graphical magnification of the dotted line of image b and extracted profile from 2D image c of HFO suggested the presence of particles size ~ 100 nm with highest probability (image d). Figure 3 shows the AFM images of CIHIO in 3D view (a and b) and 2D view including surface morphological pattern (c), indicating the rough and heterogeneous surface of the material. Extracted surface profile of the AFM image c (Fig. 3**)** shows the particles size of CIHIO is around 50 nm, which is smaller than the native HFO indicating increase possibility of surface reactivity of the material.

The surface area and pore volume of any material are very important characteristics of surface science, which have been analyzed from $N_{2(vapor)}$ adsorption-desorption profile. Figure 4 shows the $N_{2(vapor)}$ adsorption-desorption profile (plot a) including pore volume versus pore diameter (plot b). It is revealed that the specific surface area of as-prepared CIHIO was estimated to be 269.61 $m^2\ g^{-1,}$ which is about 1.6 times larger than HFO(165.60 $m^2\ g^{-1}$) (Clesceri et al. 1998), and it is consistent with the ~ 50% particle size lowering of CIHIO than HFO. The pore volume and pore diameter (Table 1) were also estimated from the plot b (Fig. 4), suggesting the material is mesoporous (pore diameter, 27.742–27.913 Å; pore width, 26.97 Å).

Powder X-ray diffraction (XRD) pattern is a good guide for identification of the crystalline mineralogical phases, if present, in a material. Thus, the XRD pattern of CIHIO taken is shown in Fig. 4c. The peaks of moderate intensities at °2 = 27.13°, 35.76°, 39.79°, 46.95°, and 56.54° indicate the presence of crystalline Fe_2O_3 phase. The peaks at 34.73° and 36.08° confirm the presence of orthorhombic crystal of FeOOH in this hybrid oxide. The peaks of moderate intensities at °2 = 34.56°, 47.26°, and 52.31° had indicated the presence of CaO in CIHIO. The size of crystallite has been calculated using Scherrer equation as described by Taghavi et al. (2018a, b) and obtained ~ 10 nm. The FTIR spectrum d of CIHIO is shown in Fig. 4 (percent transmittance versus wave number (ν, cm^{-1}) for in-depth characterization. The O–H bond stretching and bending modes obtained at $\nu = 3369.84$ cm^{-1} and ~ 1630 cm^{-1}, respectively (Deschamps et al. 2005). The absorption bands of the spectrum at ν = 1395.94 and 678.91 cm^{-1}, respectively, are vibration and bending modes of Fe–O bonds (Saha et al. 2015; Mukhopadhyay et al. 2017). Additional band at $\nu = 2374$ cm^{-1} is probably for the unsymmetrical bending of Ca–O bond and the band at ν ~ 808.72 cm^{-1} is the stretching of Ca–O bond, respectively. The pH_{zpc} of CIHIO had been analyzed using pH metric method as depicted by Babic et al. (1999) and the value is estimated to be 6.5 (Figure S2), which is very near to the neutral pH value.

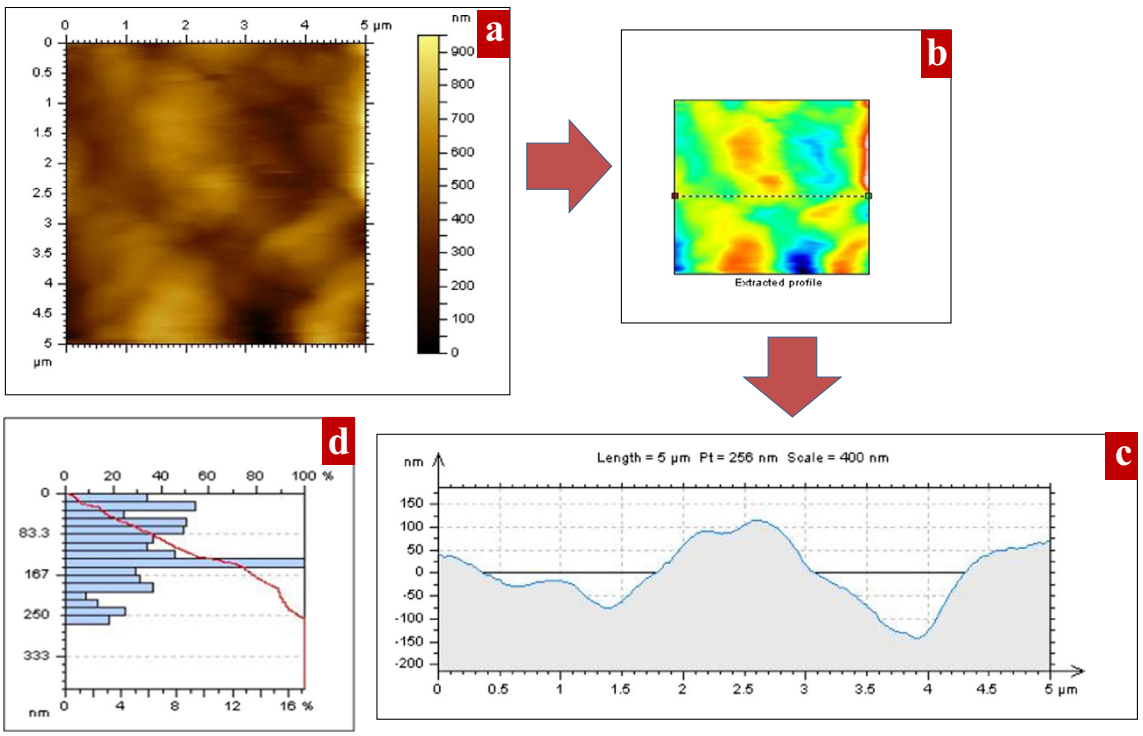

Fig. 2 **a** Atomic force microscopic image, **b** extracted profile with 2D image, **c** graphical magnification of the dotted line from the picture **b**, and **d** particle size distribution of HFO

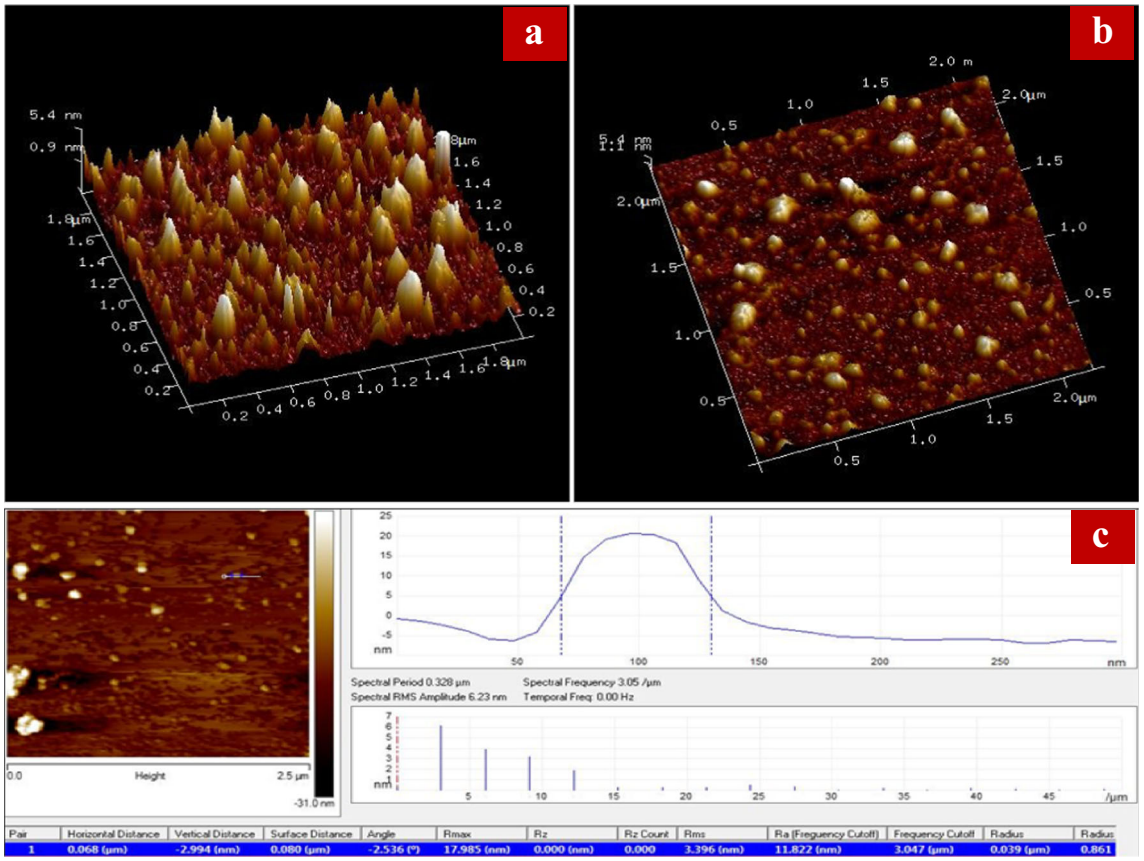

Fig. 3 Atomic force microscopic images of CIHIO in 3D **a** side view and **b** front view, **c** 2D image of CIHIO and extracted profile of a single particle

Effect of pH

The surface reaction at solid-liquid interface is highly dependent upon the solution pH, and sometimes pH plays a key role for the adsorption phenomenon. Influence of the pH_i (i = initial) on arsenite/fluoride adsorption by CIHIO was investigated in a pH_i range 3.0 to 9.0. Figure 5 demonstrates the pH dependent adsorption amount of fluoride (plot a) and arsenite (plot b) at 303 K. It can be highlighted that amount of the fluoride adsorption was nearly equal in pH_i range 3.0–7.0 showing a peak value at pH_i between 4.0 and 6.0, but amount of the arsenite adsorption was well at pH_i range 5.0–7.0 showing a peak value at pH_i 5.0. Figure 5 also reflected that more than 70% (pH_i = 3.0–7.0) of initial fluoride loading has transferred from liquid to solid surface, while more than 85% (pH_i = 5.0–7.0) of initial arsenite loading has transferred from solution to solid surfaces. The removal amount of fluoride or arsenite by CIHIO, however, declined substantially at pH_i > 7.0 due to change of the surface charge of the material (pH_{zpc} = 6.5). This result is very close to the results reported previously (Mukhopadhyay et al. 2017). The mechanism apprehended of this adsorption reaction shall be described later on in this manuscript taking help of the experimental support.

Adsorption kinetics

Kinetics of the heterogeneous adsorption process helps to predict a minimum contact time required to transfer the solute from solution to solid surface for the continuous flow system. Here, kinetics of the present adsorption reactions were monitored for C_i of solutes 5.0, 10.0, and 20.0 mg L^{-1} at pH_i 7.0 and 303 K; and also for the C_i = 10 mg L^{-1} at three different selected temperatures (288, 303, and 318 K) and pH_i 7.0. Figure 6 shows variation of the experimentally acquired kinetic data for arsenite (plot a) and fluoride (plot b) at varying solute concentrations; and also for arsenite (plot c) and fluoride (plot d) at a fixed C_i (10.0 mg L^{-1}) and the temperature 288, 303, and 318 K, respectively**.** It shows that about 80% of the initially loaded solutes have been transferred over CIHIO surface by 30 min from the starting of reaction (t = 0). Relatively a longer time was taken to transfer the residual 20% solute from solution to solid phase. It might be the consequence of steric and electrostatic repulsion between solute hosted and solute species in solution to be hosted over solid surfaces. The kinetic data displayed (Fig. 6) have been analyzed by the commonly used pseudo-first order (PFO) (Eq. 2) and pseudo-second order (PSO) models (Eq. 3) (Saha et al. 2015).

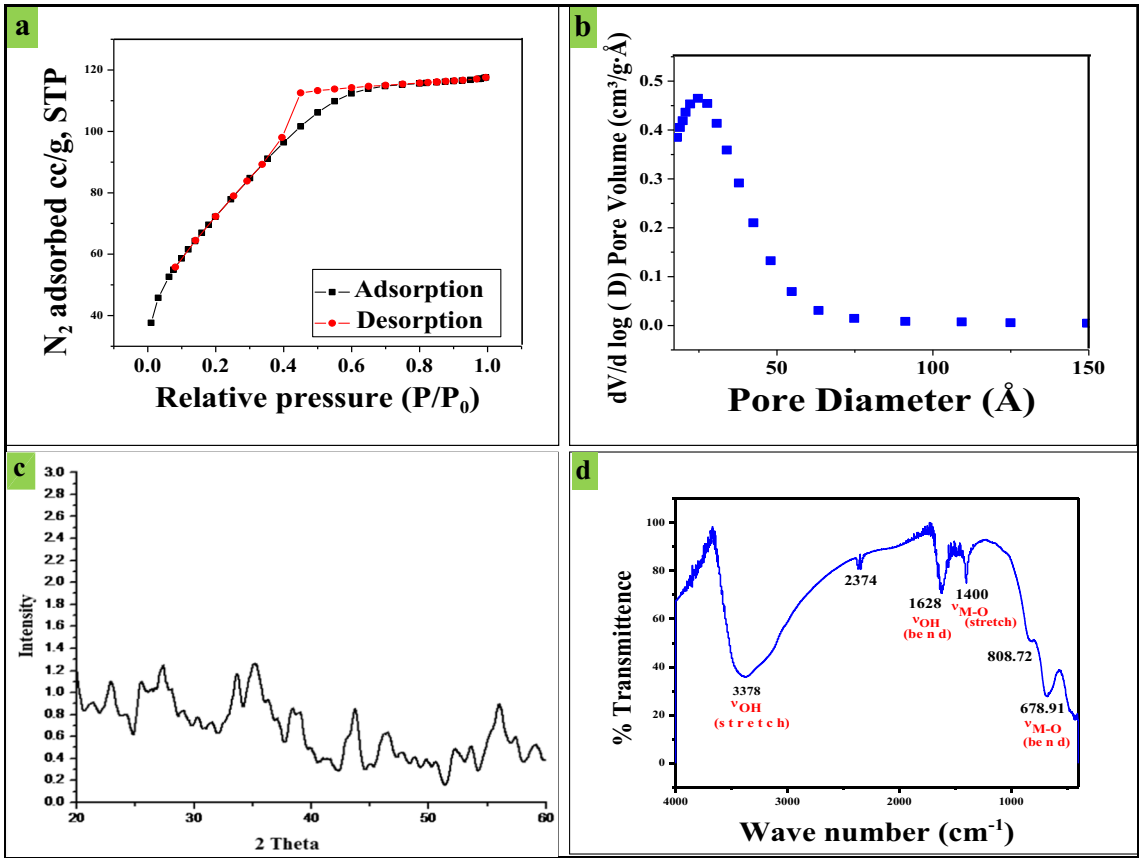

Fig. 4 **a** Nitrogen (vapor) adsorption-desorption plot for BET surface area of CIHIO; **b** pore volume versus pore diameter plot; **c** powder X-ray diffraction pattern of CIHIO; and **d** FTIR spectral plot of CIHIO

$$q_t = q_e\left(1-e^{-kt}\right) \tag{2}$$

$$q_t = \frac{(q_e)_2 k_2 t}{(1+q_e k_2 t)} \tag{3}$$

where k (min^{-1}) and k_2 (g mg^{-1}. min^{-1}) are rate constants for PFO and PSO, respectively. The significance of q_e and q_t are given elsewhere. The kinetic parameters estimated for arsenite and fluoride with non-linear model fits (Fig. 6) of the data are listed in Table 2 (different temperatures) and Table 3 (different concentrations), respectively. The weaker fit of kinetic data with the PFO equation (Eq. 2) than the PSO equation (Eq. 3) as the $q_{e(model)}$ values obtained from the PFO equation are away from the $q_{e(exp)}$values; which has also been evident from lesser R^2 and larger χ^2 values. That is, adsorption kinetics is more close to the PSO equation. Increase of the rate constant values (Table 2) with rising temperature indicates the increase of fastness of the adsorption reaction, because the solute species available has been activated to override the threshold energy for effective collision (Clesceri et al. 1998; Saha et al. 2015). Additionally, values of the q_e for arsenite increased gradually indicating the reaction is endothermic, but those for fluoride decreased favoring the reaction is exothermic (Table 2). Quite similar trends for arsenic and fluoride adsorption had been reported very recently (Gupta et al. 2008, 2010). The kinetic parameters of concentration dependent of solutes (Table 3) show that the values of rate constant for arsenite and also for fluoride increased with the increase of solute concentrations. This increase of rate constant, i.e., rate of adsorption reaction with increase of the C_i, can be justified from the increase of availability of solute per unit surface sites

Table 1 Some important characteristic parameters of CIHIO

Elemental composition (atomic %)	Fe (35.21), Ca (20.76), Cl (4.4), O (39.62)
Empirical formula	$Ca_{4.2}Fe_{7.92}O_{19.91}Cl$
Nature	Microcrystalline
Particle size (nm)	50–100
TEM image	~ 50
AFM image	
BET surface area (m^2 g^{-1})	269.61
Pore width (Å)	26.97
Pore diameter (Å)	27.742 (adsorption) 27.913 (desorption)
Pore volume (cm^3 g^{-1})	0.18
pH_{zpc}	6.5

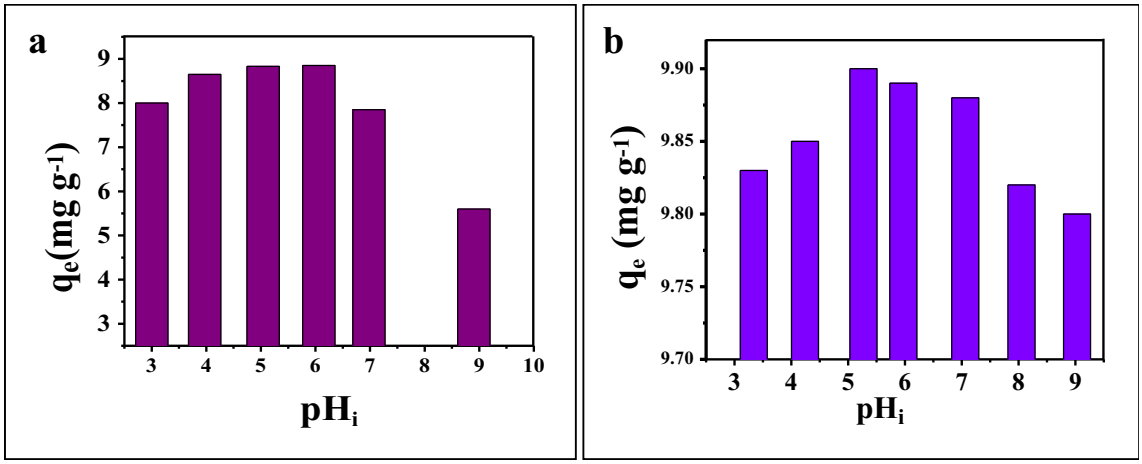

Fig. 5 Effects of the pH_i towards adsorption of **a** fluoride and **b** arsenite by CIHIO at 303 K

of material (Gupta et al. 2008; Saha et al. 2015; Mukhopadhyay et al. 2017).

Equilibrium modeling

Equilibrium study is helpful to predict the thermodynamic aspects of any reactions and adsorption mechanism. Figure 7 (q_e versus C_e) shows the equilibrium data (as points) of arsenite and fluoride adsorptions by CIHIO at temperatures 288, 303, and 318 K at pH 7.0, which have shown the rapid enhancement of q_e with increase of temperatures indicating increase of endothermic nature of the adsorption processes. These data have been modeled with most widely used isotherm equations namely Langmuir (Eq. 4) and Freundlich

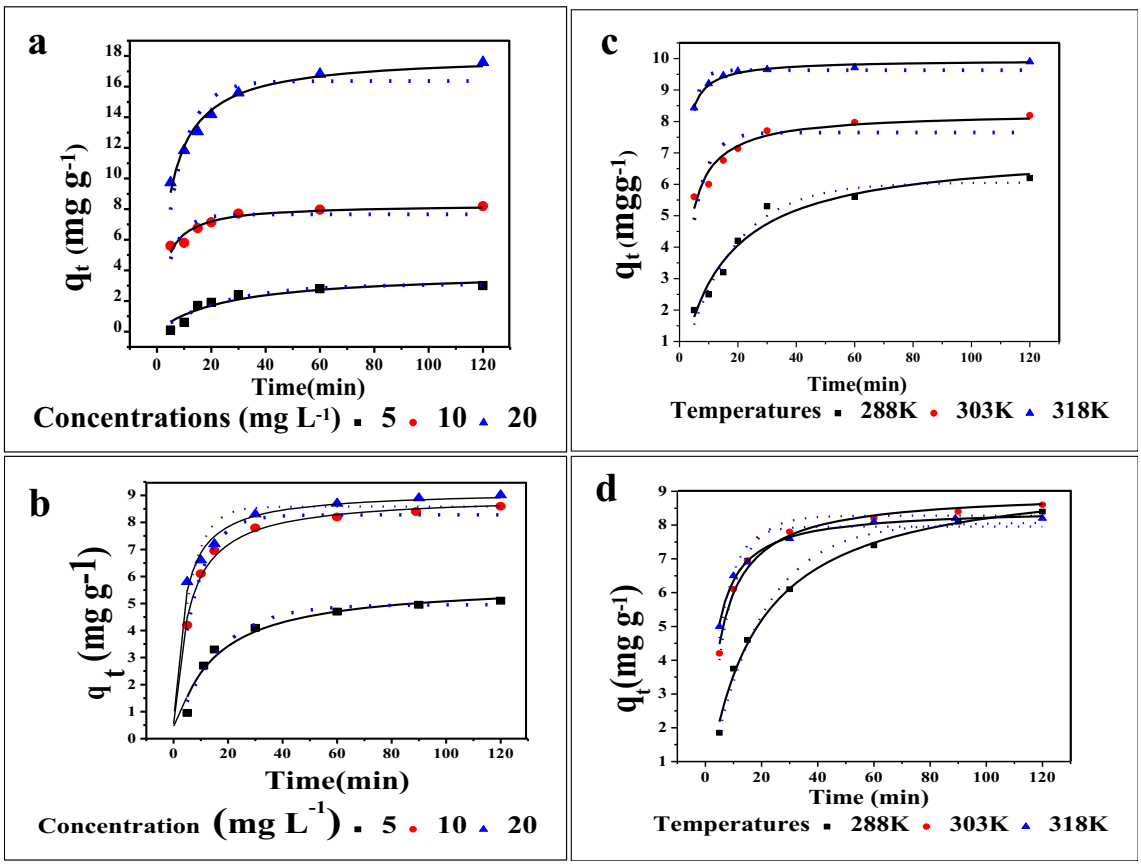

Fig. 6 The plots of q_t (mg g^{-1}) versus time of reaction, t (min) for variation of concentration of **a** arsenite and **b** fluoride; and **c** the effect of temperature on reaction kinetics for arsenite and **d** fluoride adsorption on CIHIO. Solid line indicates pseudo-second order fitting and dotted line indicate pseudo-first order model fits of data

Table 2 The parameters estimated from the model fits of kinetic data of arsenite and fluoride adsorption reactions with CIHIO at pH 7.0 (± 0.2) and temperature 288, 303, and 318 K

Adsorbate	Arsenite				Fluoride		
Kinetic models	Parameters	288 K	303 K	318 K	288 K	303 K	318 K
Pseudo-second order	k_2	0.01	0.04	0.12	0.006	0.022	0.035
(PSO)	q_e	7.12	8.29	9.95	9.59	8.983	8.492
	R^2	0.96	0.93	0.98	0.99	0.98	0.99
	χ^2	0.13	0.08	0.004	0.03	0.034	0.007
Pseudo-first	k_1	0.06	0.20	0.40	0.053	0.132	0.175
order	q_e	6.06	7.65	9.63	8.08	8.27	7.95
(PFO)	R^2	0.97	0.70	0.88	0.98	0.97	0.93
	χ^2	0.11	0.35	0.036	0.109	0.060	0.120

*C_I initial concentration (mg L^{-1}) of arsenite or fluoride, k_2 (g mg^{-1} min^{-1}), k_1 (min^{-1}), q_e (mg g^{-1})

*C_I = 10.0 mg L^{-1}

(Eq. 5) (Li et al. 2011a, b; Saha et al. 2015; Mukhopadhyay et al. 2017).

$$q_e = \frac{q_m \times b \times C_e}{1 + b \times C_e} \quad (4)$$

$$q_e = K_F \times (C_e)^{\frac{1}{n}} \quad (5)$$

Where q_e and C_e have their usual implications and mentioned earlier, q_m the maximum monolayer adsorption capacity (mg g^{-1}), b the Langmuir isotherm constant (L g^{-1}), K_F the Freundlich isotherm constant (mg g^{-1}) related to the adsorption capacity, and n is the adsorption intensity.

Figure 7 (a–d) shows the non-linear fitting of the equilibrium data with Langmuir and Freundlich isotherm models, respectively, in a and b for the arsenite and c and d for the fluoride. The isotherm parameters of related equations (4 and 5) which are estimated from the model fitting of data are given in Table 4. The parametric values inform that the fits of isotherm data were better with the Langmuir equation (R^2 = 0.97–0.99) than the Freundlich equation (R^2 = 0.90–0.97), implying adsorption sites of CIHIO are homogeneous and the tested solutes adsorption occur with monolayer surface coverage (Clesceri et al. 1998; Sivasamy et al. 2001; Addo Ntim and Mitra 2012). Goodness of the equilibrium data fitting with Langmuir isotherm has also been confirmed from the hybrid error function (HYBRID) and the Marquardt's percent standard deviation (MPSD) calculations (Table 4) using the relations as described by Sanchooli Moghaddam et al. (2016). The capacities of monolayer adsorption of Langmuir isotherm (q_m, mg g^{-1}) values are 25.57 and 29.07 at 303 K for fluoride and arsenite, respectively. With increase of the temperature, values of the q_m of CIHIO are increased for both arsenite and fluoride, indicating endothermic nature of the reactions (Gupta et al. 2007, 2010; Ghosh et al. 2014). Thus, the accessible adsorption sites by solutes over CIHIO have increased with increasing temperature, and the adsorption capacities enhanced. The dimensionless parameter, K_L which is also called separation factor

Table 3 The kinetic parameters estimated from the model fits of kinetic data of arsenite and fluoride adsorption reactions with CIHIO at pH 7.0 (± 0.2) and temperature 288 K

Adsorbate	Arsenite *C_I (mg L^{-1})				Fluoride *C_I (mg L^{-1})		
Kinetic model	Kinetic parameters	5.0	10.0	20.0	5.0	10.0	20.0
Pseudo-second order (PSO)	k_2	0.01	0.04	0.06	0.012	0.022	0.032
	q_e	3.91	8.30	18.06	5.78	8.98	9.16
	R^2	0.89	0.91	0.98	0.97	0.98	0.97
	χ^2	0.15	0.16	0.19	0.095	0.034	0.053
Pseudo-first	k_1	0.04	0.13	0.19	0.064	0.132	0.173
order (PFO)	q_e	3.09	7.66	16.36	4.95	8.27	8.58
	R^2	0.92	0.68	0.84	0.96	0.97	0.81
	χ^2	0.04	0.19	0.13	0.064	0.060	0.361

*C_I: initial concentration (mg L^{-1}) of arsenite or fluoride, k_2 (g mg^{-1} min^{-1}), k_1 (min^{-1}), q_e (mg g^{-1})

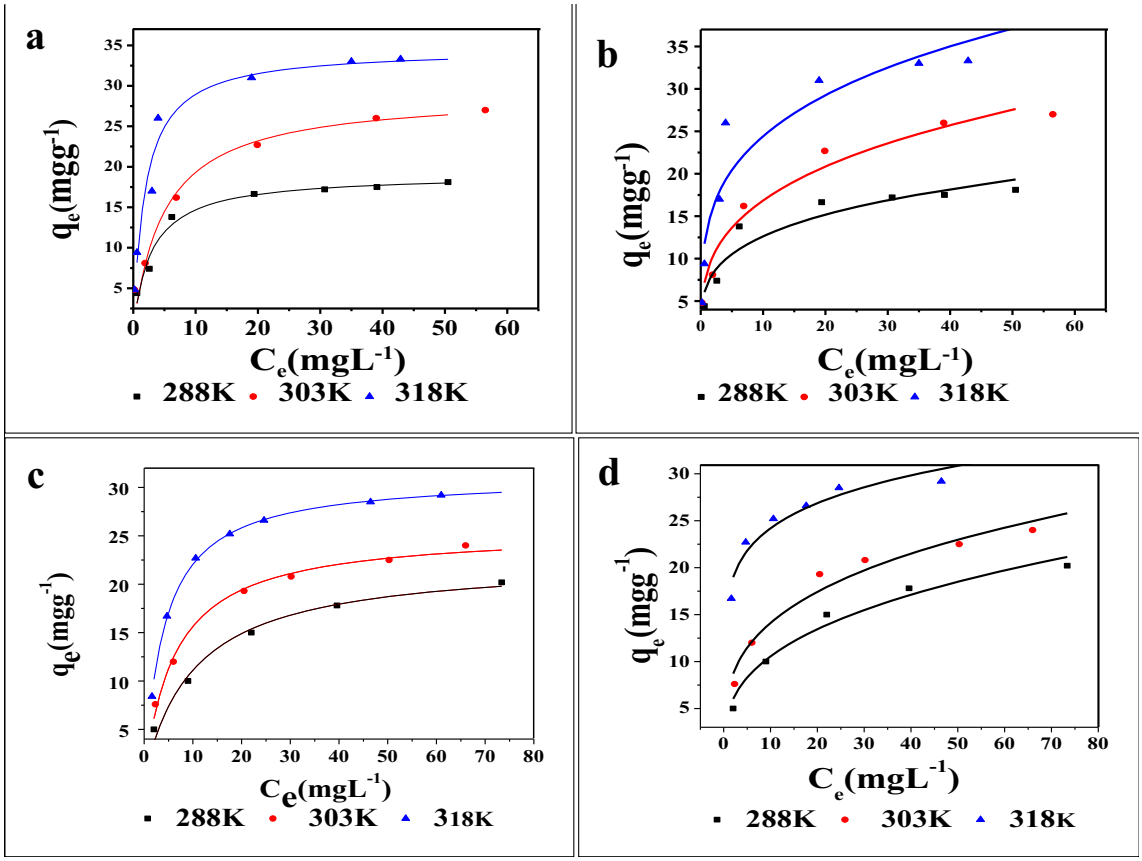

Fig. 7 The equilibrium data fit with the **a** Langmuir isotherm, **b** Freundlich isotherm for the arsenite adsorption; the **c** Langmuir isotherm and the **d** Freundlich isotherm for the fluoride adsorption by CIHIO at different temperatures

highlights an obligatory feature of the Langmuir isotherm and can be calculated by the relation (Eq. 6).

$$K_L = \frac{1}{1 + b \times C_i} \tag{6}$$

where b is the Langmuir constant (L mg^{-1}) and the significance of C_i is given elsewhere. If the value of K_L is (a) ranged between 0.0 and 1.0, the reaction is favorable; (b) greater than unity, the reaction is unfavorable, and (c) $K_L = 1$, the reaction is irreversible (Hall et al. 1966). Here, values of the K_L ranged

Table 4 Non-linear isotherm model fit parameters for arsenite and fluoride adsorption by CIHIO at pH 7.0 (± 0.2) at temperatures 288, 303, and 318 K (C_i range, 5.0–80.0 mg L^{-1})

Adsorbate		Arsenite			Fluoride		
Isotherm models	Isotherm model fit parameters	288 K	303 K	318 K	288 K	303 K	318 K
Langmuir	q_m	19.06	29.07	34.56	22.57	25.57	31.14
	b	0.330	0.201	0.520	0.096	0.157	0.242
	R^2	0.97	0.97	0.97	0.98	0.99	0.99
	χ^2	0.92	2.87	5.52	0.78	0.36	0.040
	HYBRID	2.71	0.403	0.536	0.581	0.733	0.009
	MPSD	16.46	6.34	8.55	7.62	8.56	0.94
Freundlich	K_F	6.92	8.37	13.43	4.73	7.06	11.16
	n	3.82	3.28	3.85	2.87	3.31	3.97
	R^2	0.91	0.97	0.90	0.97	0.96	0.89
	χ^2	3.27	3.00	15.80	1.25	1.89	7.33
	HYBRID	12.75	10.45	16.64	5.18	9.34	16.17
	MPSD	35.70	32.32	40.79	22.75	30.56	40.21

q_m (mg g^{-1}), b (L mg^{-1}), K_F (mg$^{1-1/n}$ L$^{1/n}$ g^{1})

Table 5 A comparative list of monolayer capacity of CIHIO for adsorption of arsenite and fluoride with some similar type of iron-based adsorbent material at a temperature 303 K

Arsenite				Adsorbent materials	Fluoride			
Reference	C_i range (mg L^{-1})	q_m (mg g^{-1})	pH		pH	q_m (mg $g^{-1)}$	C_i range (mg L^{-1})	Reference
Present work	5–100	29.07	7.0	CIHIO	6.9	25.52	5–100	Present work
Mohan and Pittman (2007)	5–250	25.00	7.0	Granular ferric hydroxide	6.8	7.0	1–100	Manna et al. (2003)
Gupta et al. (2008)	5–250	64.5	7.0	Fe(III)–Zr(IV) mixed oxide	6.8	8.21	5–50	Biswas et al. (2007a, b)
Basu and Ghosh (2011)	5–250	58.30	7.0	Fe–Al mixed oxide	6.9	17.73	5–50	Biswas et al. (2007a, b)
Ghosh et al. (2006)	5–500	43.86	7.0	Fe–Sn mixed oxide	6.4	10.47	10–50	Biswas et al. (2009)
Basu et al. (2010)	5–250	10.404	7.0	Fe–Cr mixed oxide	6.5	16.34	10–50	Biswas et al. (2010)
Manna et al. (2003)	5–250	33.33	7.0	Crystalline hydrous ferric oxide	7.0	16.50	5.0–50.0	Dey et al. (2004)

C_i = initial concentration of arsenite/fluoride for adsorption reaction with CIHIO

between 0 and 1.0 even at $C_i = 0.01$ mg L^{-1} of the tested ions, indicating the highly favorable adsorption processes.

In order to compare the removal efficiency, values of the q_m for arsenite and fluoride adsorption by CIHIO have been compared with other iron based materials in Table 5 (Manna et al. 2003; Dey et al. 2004; Ghosh et al. 2006; Mohan and Pittman 2007; Biswas et al. 2007a, b; Gupta et al. 2008; Kumar et al. 2009; Biswas et al. 2009, 2010; Basu et al. 2010; Basu and Ghosh 2011). This comparison of q_m has a little significance unless the experimental parameters such as concentration range of solute, adsorbent dose, and agitation speed are identical. However, values of the q_m of CIHIO are quite high than some of the materials reported such as iron(III) oxide and iron(III) based mixed oxides (Table 5).

Thermodynamics parameters

Evaluation of the thermodynamic parameters is particularly important to estimate the spontaneity of adsorption reactions. Thus, the parameters such as the changes of Gibb's free energy (ΔG^0), entropy (ΔS^0), and enthalpy (ΔH^0) under the standard states can be estimated by the relations (Eqs. 7–9) (Viswanathan et al. 2009; Saha et al. 2014; Ghosh et al. 2014; Li et al. 2017; Mukhopadhyay et al. 2017) below:

$$\Delta G^0 = -RTlnK_c \quad (7)$$

$$\Delta G^0 = \Delta H^0 - T\Delta S^0 \quad (8)$$

$$lnK_c = \frac{\Delta S^0}{R} - \frac{\Delta H^0}{RT} \quad (9)$$

where R is an ideal gas constant (8.314 J mol^{-1} K^{-1}), K_c, the equilibrium constant at a temperature T, can be calculated by $K_c = q_e \frac{}{C_e}$ where $q_e \frac{}{C_e}$ is called the adsorption affinity which was calculated as calculated by Frantz et al. (2017), Milonlic (2007), and Cadaval Jr et al. (2015). Assuming $\Delta S^0$and $\Delta H^0$are to be constant at the range of working temperature, the values calculated from slope and intercept of the plot of ln (q_e/C_e) against 1/T (Figure S3) were used to calculate the ΔG^0 at temperatures studied using the Eq. 7. The values obtained for ΔG^0, ΔS^0, and ΔH^0 are recorded in Table 6. The positive value of the ΔH^0 has thus supported that the arsenite and fluoride adsorption by CIHIO inclined to endothermic. Again, the positive values of ΔS^0 for arsenite and also fluoride adsorption by the present material confirm the increase of chaotic nature at solid-liquid interface owing to the release of aqua molecules when hydrated solute was hosted by the solid surface. Influence of the entropy change is so high that the influence of enthalpy change has been overturned to have the value of ΔG^0 negative and the adsorption reactions become spontaneous. Increase of the temperature has increased the magnitude of ΔG^0, indicating the increase of spontaneity of the adsorption processes (Gupta et al. 2007, 2010).

Table 6 Estimated thermodynamic parameter for arsenite and fluoride adsorption by CIHIO

Contagions	*C_i (mg L^{-1})	ΔH^0 (kJ mol^{-1})	ΔS^0 (J mol^{-1} K^{-1})	ΔG^0 (kJ mol^{-1}) at Temperature (K)		
				288	303	318
Arsenite	10.0	+ 2.14	+ 70.60	− 18.02	− 19.07	− 20.12
Fluoride	10.0	+ 29.28	+ 102.43	− 0.2523	− 1.746	− 3.352

*C_i = initially loaded arsenite or fluoride concentration for adsorption reaction with CIHIO

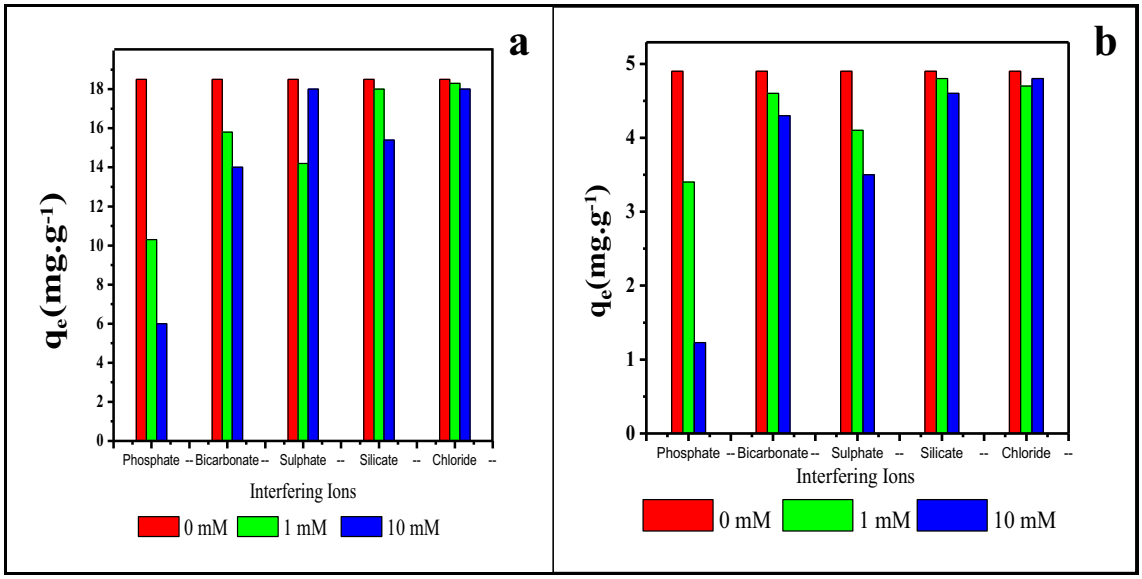

Fig. 8 The effects of co-occurring ions on **a** arsenite and **b** fluoride adsorptions by CIHIO

Effect of some groundwater occurring ions

Field trial is impractical for decontamination of the target ions from water without acquiring knowledge of the adverse influence of major ions occurring in the ground water. Thus, the arsenite and fluoride adsorption reactions with CIHIO were investigated separately in presence of PO_4^{3-}, HCO_3^-, SiO_3^{2-}, Cl^-, and SO_4^{2-}. The results are shown in plot a (arsenite) and plot b (fluoride) in Fig. 8. It shows sharp decline of removal efficiency of both arsenite and fluoride in the presence of PO_4^{3-} ion (Viswanathan et al. 2009; Li et al. 2017). Like the PO_4^{3-}, HCO_3^-, and SO_4^{2-} ions also reduced the removal efficiency of this material but did this job somewhat less efficiently than PO_4^{3-} (Mukhopadhyay et al. 2017). The chloride ion has no significant adverse influence on the adsorption reactions of arsenite and fluoride with CIHIO. The arsenite removal efficiency of CIHIO is thus reduced as $PO_4^{3-} > HCO_3^- > SiO_3^{2-} > SO_4^{2-} > Cl^-$ when each was at a level of 10 mM per L. The order mentioned above in removing the arsenite has been modified somewhat as $PO_4^{3-} > SO_4^{2-} > HCO_3^- > SiO_3^{2-} > Cl^-$ when the ions level was 1 mM per L. The results showed that the phosphate has parallel competition for the solid surface with arsenite, and drastically cuts the adsorption sites of solid surface for arsenite or fluoride adsorption (Kumar et al. 2009; Basu and Ghosh 2011; Ghosh et al. 2014). Like the arsenite, the fluoride adsorption by CIHIO was also notably cut in the sequence as $PO_4^{3-} > SO_4^{2-} > HCO_3^- > SiO_3^{2-} > Cl^-$ when the foreign ion concentration was at a level of 1.0 mM or 10 mM per L with fluoride solution. The adverse effect of phosphate on the fluoride removal had also been reported for adsorbents such as granular ferric oxide (Kumar et al. 2009), chitosan bead (Biswas et al.

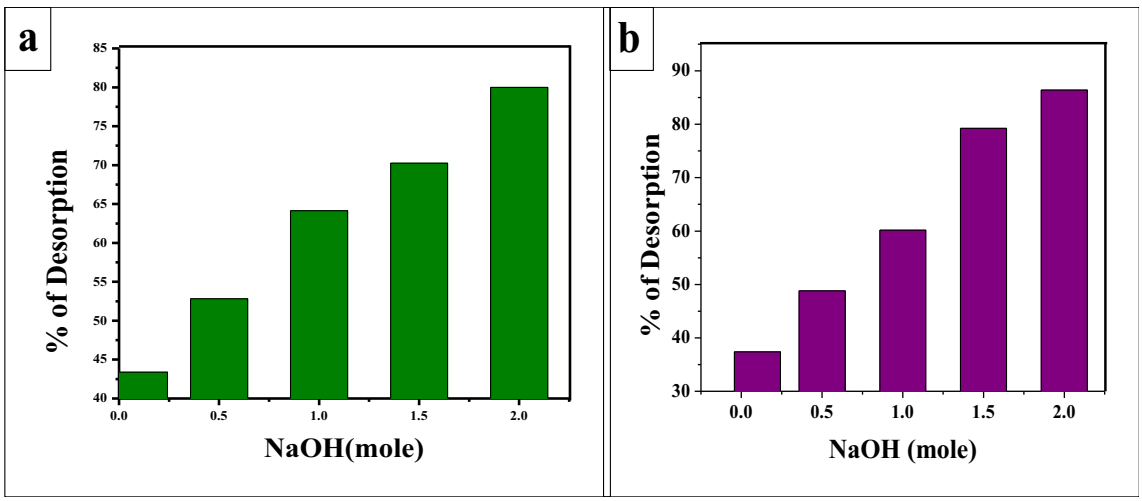

Fig. 9 The desorption percentages of **a** arsenite and **b** fluoride as bar graphs against the molarity of NaOH solution

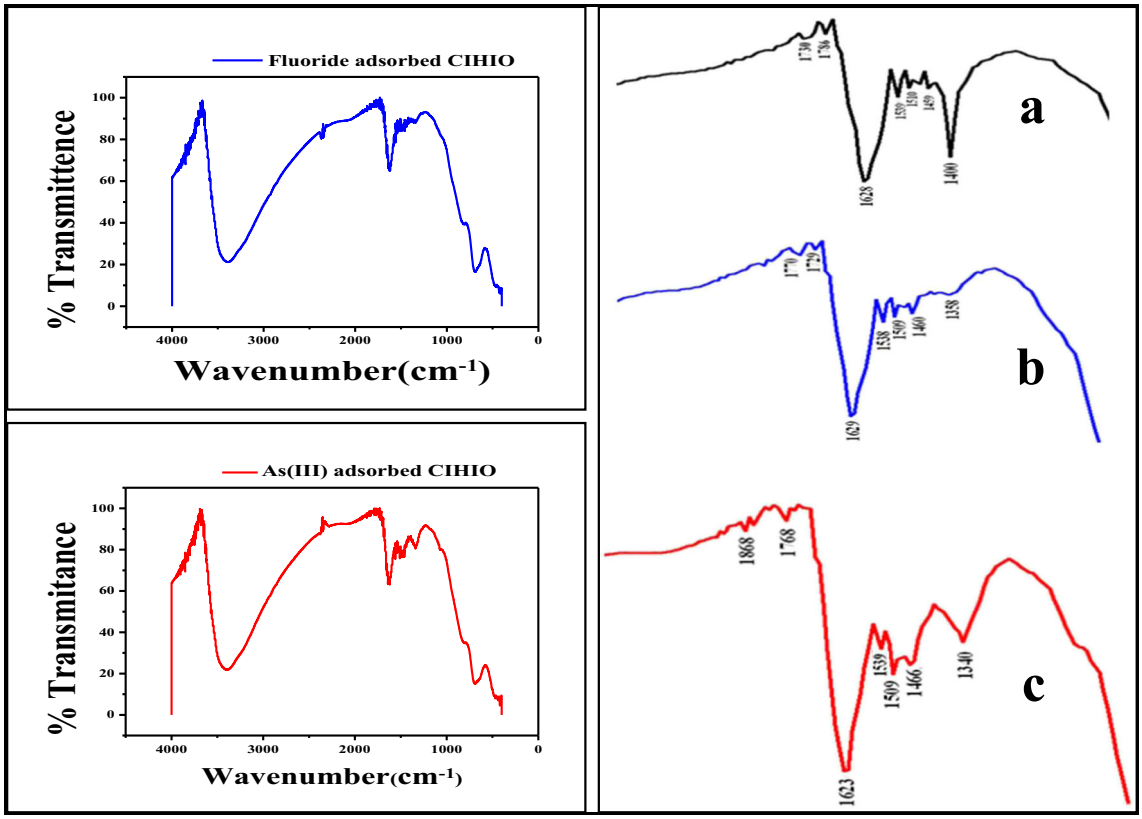

Fig. 10 The FTIR spectra (% transmission versus wave number) of fluoride-adsorbed and arsenite-adsorbed CIHIO, and **b** selected portion of fluoride-adsorbed and **c** arsenite-adsorbed spectra in a comparing with that of **a** CIHIO spectra

2010), and Al-Ce mixed oxide (Liu et al. 2010). It is fortunate that the phosphate concentration in groundwater is much lower than 1.0 mM per L (Ghosh et al. 2014). The sulfate ion did the same job but somewhat less strongly than the phosphate ion.

Regeneration of spent adsorbent

Recycling of an adsorbent material is dependent upon regain its activity via regeneration with a suitable reagent of the spent material. Hence, the adsorption activity regain by spent CIHIO was investigated through desorption of the adsorbed species from the adsorbent surface. Figure 9 shows the results as percent desorption of arsenic (plot a) and fluoride (plot b) against molar concentration of the NaOH solution. It shows the increase of percent desorption with increasing molar strength of NaOH solution. The desorption percentages increased noticeably to 80–85% with increasing molar strength of NaOH to 2.0 M. This high desorption percentage (80–85%) is a strong indication signal in favor of weak interaction between adsorbate and adsorbent (Gupta et al. 2008). As the

Scheme 1 Proposed surface reaction mechanism for arsenite/fluoride uptake by CIHIO

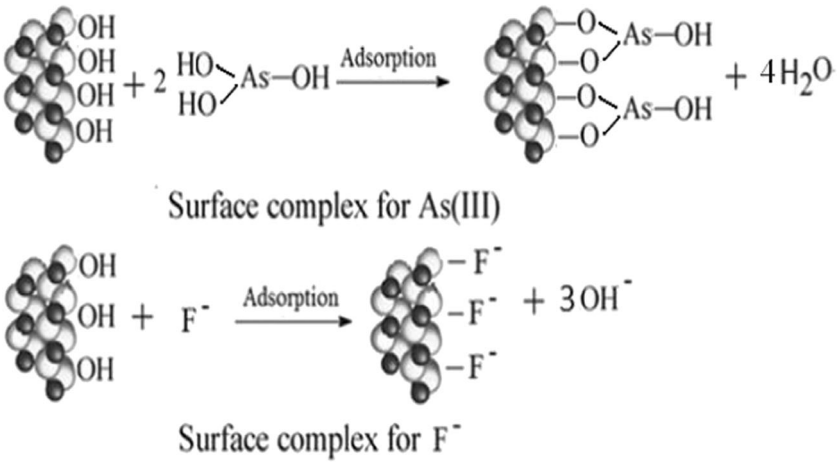

adsorption reactions of arsenite and fluoride with CIHIO were endothermic indicating the low activation energy for desorption and possibility of high desorption percentage. It is found experimentally that the CIHIO has regained its adsorption efficiency by ~ 60–65% for both arsenic and fluoride adsorption even after the fifth stage of desorption of the spent material, indicating possibility of commercial viability of CIHIO.

Adsorption mechanism

Figure 10 shows the FTIR spectra of pristine CIHIO, fluoride adsorbed and arsenite adsorbed CIHIO separately. The fluoride adsorption by the material takes place with increase of equilibrium solution pH, supporting the replacement of OH^- from the solid surface with F^-adsorption (Gupta et al. 2008; Patel et al. 2009; Liu et al. 2010; Ghosh et al. 2014), which has been confirmed from disappearance of the M–O stretching band at a wave number (υ) 1400 cm^{-1}. Instead, a weak band appeared at υ = 1406 cm^{-1} for M–F stretching, which is similar to the report that was made by Liu et al. (2010). The weak band at 1358 cm^{-1} in fluoride adsorbed material is possibly for existence of the trace M–OH group still retained with a shift of nearly 40 cm^{-1} which is possibly due to hydrogen bonding with fluoride (Fornaro et al. 2015). The remaining bands between 1400 and 1628 cm^{-1} are retained with very small shift in the fluoride adsorbed material. However, the retention of more intense FTIR stretching band of hydroxyl group at 3400–3500 cm^{-1} of the fluoride adsorbed material (Li et al. 2010) instead of disappearing is possibly due to hydration of surface metal ions via co-ordination from the aqueous solution.

However, the adsorption of arsenite by CIHIO takes place somewhat differently from that of fluoride. The stretching band in FTIR spectra of pristine material at a υ value 3378 cm^{-1} shifted to 3386 cm^{-1}, which moves slightly to the higher υ value with intensity increase of the band. This might be for the enhanced physically adsorbed water (Li et al. 2010). The bending O–H band at a υ = 1622 cm^{-1} became more intense in arsenite adsorbed material compared to the pristine material. However, the M–O stretching band of pristine material at υ = 1400 cm^{-1} split up to three bands (1337, 1461, and 1507 cm^{-1}) with decrease of band intensity in arsenite adsorbed material which is different from the report made by Li et al. (Rongshu et al. 1995; Li et al. 2010). This is presumably due to the chelation of $As(OH)_3$ on the metal oxide surface and, thus the characteristic As–OH band appears around 800 cm^{-1} in the arsenite adsorbed IR spectra. This is not prominently mentionable due to noisy overlapping of bands in the lower side of wave number region (Gupta et al. 2010; Fornaro et al. 2015). Based on the above analyses of equilibrium solution pH and FTIR spectroscopy of spent materials, the mechanism of arsenite/fluoride adsorption has been depicted in Scheme 1 below:

Conclusion

Analytically calcium-incorporated hydrous iron(III) oxide (CIHIO) has been established as a material of microcrystalline and mesoporous nature with pH_{zpc} ~ 6.5 and irregular surface morphology. The surface area is notably larger than hydrous ferric oxide only. This material when used for the adsorption of arsenite/fluoride with change of contact time from their aqueous solution at optimized pH shows the reaction kinetics of pseudo-second order type. The adsorption equilibrium agrees well to the Langmuir monolayer adsorption mechanism with encouragingly high monolayer capacity for both arsenite and fluoride. Highly spontaneous adsorption processes are the consequence of favorable entropy changes. High desorption (80–85%) percentages with 2.0 M of aqueous NaOH from the spent CIHIO surfaces has indicated reuse possibility of CIHIO. Repeating the use of this material shows that high (60–65%) adsorption efficiency is retained even after fourth stage of recycle. The phosphate ion even at a level of 1 mM per L is capable to reduce the adsorption efficiency of CIHIO. The adsorption mechanism for the arsenite was established to be surface complex reaction while that for the fluoride was ion-exchange type.

Acknowledgement The authors are grateful to the Principal, Maharaja Manindra Chandra College for providing laboratory facilities, and Presidency University for extending some research facilities. One of the authors (KB) is thankful to UGC for the financial support [F.PSW-087/15-16 (ERO)] of this work, and PS is thankful to W.B. State DHESTBT [211(Sanc.)/ST/P/S&T/15G-14/2017] for financial support.

References

Addo Ntim S, Mitra S (2012) Adsorption of arsenic on multiwall carbon nanotube–zirconia nanohybrid for potential drinking water purification. J Colloid Interface Sci 375:154–159. https://doi.org/10.1016/j.jcis.2012.01.063

Ali I (2012) New generation adsorbents for water treatment. Chem Rev 112:5073–5091. https://doi.org/10.1021/cr300133d

Babel S (2003) Low-cost adsorbents for heavy metals uptake from contaminated water: a review. J Hazard Mater 97:219–243. https://doi.org/10.1016/S0304-3894(02)00263-7

Babic BM, Milonjic JM, Kaludierovic VB (1999) Point of zero charge and intrinsic equilibrium constants of activated carbon cloth. Carbon 37:477–481

Basu T, Ghosh UC (2011) Arsenic(III) removal performances in the absence/presence of groundwater occurring ions of agglomerated Fe(III)–Al(III) mixed oxide nanoparticles. J Ind Eng Chem 17:834–844. https://doi.org/10.1016/j.jiec.2011.09.002

Basu T, Gupta K, Ghosh UC (2010) Equilibrium and thermodynamics on arsenic(III) sorption reaction in the presence of background ions occurring in groundwater with nanoparticle agglomerates of hydrous iron(III) + chromium(III) mixed oxide †. J Chem Eng Data 55:2039–2047. https://doi.org/10.1021/je901010x

Biswas K, Bandhoyapadhyay D, Ghosh UC (2007a) Adsorption kinetics of fluoride on iron(III)-zirconium(IV) hybrid oxide. Adsorption 13:83–94. https://doi.org/10.1007/s10450-007-9000-1

Biswas K, Saha SK, Ghosh UC (2007b) Adsorption of fluoride from aqueous solution by a synthetic iron(III)−Aluminum(III) mixed oxide. Ind Eng Chem Res 46:5346–5356. https://doi.org/10.1021/ie061401b

Biswas K, Gupta K, Ghosh UC (2009) Adsorption of fluoride by hydrous iron(III)–tin(IV) bimetal mixed oxide from the aqueous solutions. Chem Eng J 149:196–206. https://doi.org/10.1016/j.cej.2008.09.047

Biswas K, Debnath S, Ghosh UC (2010) Physicochemical aspects on fluoride adsorption for removal from water by synthetic hydrous iron(III) – chromium(III) mixed oxide. Sep Sci Technol 45:472–485. https://doi.org/10.1080/01496390903526667

Cadaval TRS Jr, Dotto GL, Pinto LAA (2015) Equilibrium isotherms, thermodynamics and kinetic studies for the adsorption of food azo dyes onto chitosan films. Chem Eng Commun 202:1316–1323. https://doi.org/10.1080/00986445.2014.934449

Cao C-Y, Cui Z-M, Chen C-Q et al (2010) Ceria hollow nanospheres produced by a template-free microwave-assisted hydrothermal method for heavy metal ion removal and catalysis. J Phys Chem C 114:9865–9870. https://doi.org/10.1021/jp101553x

Chandra V, Park J, Chun Y et al (2010) Water-dispersible magnetite-reduced graphene oxide composites for arsenic removal. ACS Nano 4:3979–3986. https://doi.org/10.1021/nn1008897

Chaturvedi AK, Yadava KP, Pathak KC, Singh VN (1990) Defluoridation of water by adsorption on fly ash. Water Air Soil Pollut 49:51–61. https://doi.org/10.1007/BF00279509

Chen L, He B-Y, He S et al (2012) Fe—Ti oxide nano-adsorbent synthesized by co-precipitation for fluoride removal from drinking water and its adsorption mechanism. Powder Technol 227:3–8. https://doi.org/10.1016/j.powtec.2011.11.030

Clesceri LS, American Public Health Association, American Water Works Association, Water Pollution Control Federation (eds) (1998) Standard methods: for the examination of water and wastewater, 20th. edn. American Public Health Ass, Washington

Crittenden JC, Borchardt JH, Harza MW (eds) (2012) MWH's water treatment: principles and design, 3rd. edn. Wiley, Hoboken

Deschamps E, Ciminelli VST, Höll WH (2005) Removal of As(III) and As(V) from water using a natural Fe and Mn enriched sample. Water Res 39:5212–5220. https://doi.org/10.1016/j.watres.2005.10.007

Dey S, Goswami S, Ghosh UC (2004) Hydrous ferric oxide (HFO)—a scavenger for fluoride from contaminated water. Water Air Soil Pollut 158:311–323. https://doi.org/10.1023/B:WATE.0000044854.71497.b6

Fallahzadeh RA, Miri M, Taghavi M et al (2018) Spatial variation and probabilistic risk assessment of exposure to fluoride in drinking water. Food Chem Toxicol 113:314–321. https://doi.org/10.1016/j.fct.2018.02.001

Fan X (2003) Adsorption kinetics of fluoride on low cost materials. Water Res 37:4929–4937. https://doi.org/10.1016/j.watres.2003.08.014

Fornaro T, Burini D, Biczysko M, Barone V (2015) Hydrogen-bonding effects on infrared spectra from anharmonic computations: uracil–water complexes and uracil dimers. J Phys Chem A 119:4224–4236. https://doi.org/10.1021/acs.jpca.5b01561

Frantz TS, Silveira N Jr, Quadro MS, Andreazza R, Barcelos AA, Cadaval TRS Jr, Pinto LAA (2017) Cu(II) adsorption from copper mine water by chitosan films and the matrix effects. Environ Sci Pollut Res 24:5908–5917. https://doi.org/10.1007/s11356-016-8344-z

Ghosh UC, Bandyopadhyay D, Manna B, Mandal M (2006) Hydrous Iron(III)-Tin(IV) Binary mixed oxide: arsenic adsorption behaviour from aqueous solution. Water Quality Research Journal 41:198–209. https://doi.org/10.2166/wqrj.2006.023

Ghosh A, Chakrabarti S, Biswas K, Ghosh UC (2014) Agglomerated nanoparticles of hydrous Ce(IV)+Zr(IV) mixed oxide: preparation, characterization and physicochemical aspects on fluoride adsorption. Appl Surf Sci 307:665–676. https://doi.org/10.1016/j.apsusc.2014.04.095

Gupta VK, Ali I, Saini VK (2007) Defluoridation of wastewaters using waste carbon slurry. Water Res 41:3307–3316. https://doi.org/10.1016/j.watres.2007.04.029

Gupta K, Biswas K, Ghosh UC (2008) Nanostructure iron(III)−zirconium(IV) binary mixed oxide: synthesis, characterization, and physicochemical aspects of arsenic(III) sorption from the aqueous solution. Ind Eng Chem Res 47:9903–9912. https://doi.org/10.1021/ie8002107

Gupta K, Maity A, Ghosh UC (2010) Manganese associated nanoparticles agglomerate of iron(III) oxide: synthesis, characterization and arsenic(III) sorption behavior with mechanism. J Hazard Mater 184:832–842. https://doi.org/10.1016/j.jhazmat.2010.08.117

Gupta VK, Ali I, Saleh TA et al (2012) Chemical treatment technologies for waste-water recycling—an overview. RSC Adv 2:6380. https://doi.org/10.1039/c2ra20340e

Hall KR, Eagleton LC, Acrivos A, Vermeulen T (1966) Pore- and solid-diffusion kinetics in fixed-bed adsorption under constant-pattern conditions. Ind Eng Chem Fundam 5:212–223. https://doi.org/10.1021/i160018a011

Jing C, Cui J, Huang Y, Li A (2012) Fabrication, characterization, and application of a composite adsorbent for simultaneous removal of arsenic and fluoride. ACS Appl Mater Interfaces 4:714–720. https://doi.org/10.1021/am2013322

Ku Y, Chiou H-M (2002) The adsorption of fluoride ion from aqueous solution by activated alumina. Water Air Soil Pollut 133:349–361. https://doi.org/10.1023/A:1012929900113

Kumar E, Bhatnagar A, Ji M et al (2009) Defluoridation from aqueous solutions by granular ferric hydroxide (GFH). Water Res 43:490–498. https://doi.org/10.1016/j.watres.2008.10.031

Lai YD, Liu JC (1996) Fluoride removal from water with spent catalyst. Sep Sci Technol 31:2791–2803. https://doi.org/10.1080/01496399608000827

Li Z, Deng S, Yu G et al (2010) As(V) and As(III) removal from water by a Ce–Ti oxide adsorbent: behavior and mechanism. Chem Eng J 161:106–113. https://doi.org/10.1016/j.cej.2010.04.039

Li H, Li W, Zhang Y et al (2011a) Chrysanthemum-like α-FeOOH microspheres produced by a simple green method and their outstanding ability in heavy metal ion removal. J Mater Chem 21:7878. https://doi.org/10.1039/c1jm10979k

Li W, Cao C-Y, Wu L-Y et al (2011b) Superb fluoride and arsenic removal performance of highly ordered mesoporous aluminas. J Hazard Mater 198:143–150. https://doi.org/10.1016/j.jhazmat.2011.10.025

Li M, Wang C, O'Connell MJ, Chan CK (2015) Carbon nanosphere adsorbents for removal of arsenate and selenate from water. Environ Sci Nano 2:245–250. https://doi.org/10.1039/C4EN00204K

Li W, Chen D, Xia F et al (2016) Extremely high arsenic removal capacity for mesoporous aluminium magnesium oxide composites. Environ Sci Nano 3:94–106. https://doi.org/10.1039/C5EN00171D

Li J, Gyoten H, Sonoda A et al (2017) Removal of trace arsenic to below drinking water standards using a Mn–Fe binary oxide. RSC Adv 7:1490–1497. https://doi.org/10.1039/C6RA26806D

Liu H, Deng S, Li Z et al (2010) Preparation of Al–Ce hybrid adsorbent and its application for defluoridation of drinking water. J Hazard Mater 179:424–430. https://doi.org/10.1016/j.jhazmat.2010.03.021

Maliyekkal SM, Sharma AK, Philip L (2006) Manganese-oxide-coated alumina: a promising sorbent for defluoridation of water. Water Res 40:3497–3506. https://doi.org/10.1016/j.watres.2006.08.007

Manna BR, Dey S, Debnath S, Ghosh UC (2003) Removal of arsenic from groundwater using crystalline hydrous ferric oxide (CHFO). Water Qual Res J Can 38:193–210. https://doi.org/10.2166/wqrj.2003.013

Mayadevi S (1996) Adsorbents for the removal of fluoride from water. Ind Chem Engg Sect A 38:155–157

Medellin-Castillo NA, Leyva-Ramos R, Ocampo-Perez R et al (2007) Adsorption of fluoride from water solution on bone char. Ind Eng Chem Res 46:9205–9212. https://doi.org/10.1021/ie070023n

Milonlic SK (2007) A consideration of the correct calculation of thermodynamic parameters of adsorption. J Serb Chem Soc 72(12):1363–1367. https://doi.org/10.2298/JSC0712363M

Miri M, Bhatnagar A, Mahdavi Y et al (2018) Probabilistic risk assessment of exposure to fluoride in most consumed brands of tea in the Middle East. Food Chem Toxicol 115:267–272. https://doi.org/10.1016/j.fct.2018.03.023

Mohan D, Pittman CU (2007) Arsenic removal from water/wastewater using adsorbents—a critical review. J Hazard Mater 142:1–53. https://doi.org/10.1016/j.jhazmat.2007.01.006

Mukhopadhyay K, Ghosh A, Das SK et al (2017) Synthesis and characterisation of cerium(IV)-incorporated hydrous iron(III) oxide as an adsorbent for fluoride removal from water. RSC Adv 7:26037–26051. https://doi.org/10.1039/C7RA00265C

Patel G, Pal U, Menon S (2009) Removal of fluoride from aqueous solution by CaO nanoparticles. Sep Sci Technol 44:2806–2826. https://doi.org/10.1080/01496390903014425

Paul B, Parashar V, Mishra A (2015) Graphene in the Fe $_3$ O $_4$ nanocomposite switching the negative influence of humic acid coating into an enhancing effect in the removal of arsenic from water. Environ Sci: Water Res Technol 1:77–83. https://doi.org/10.1039/C4EW00034J

Pendergast MM, Hoek EMV (2011) A review of water treatment membrane nanotechnologies. Energy Environ Sci 4:1946. https://doi.org/10.1039/c0ee00541j

Raichur A, Jyoti Basu M (2001) Adsorption of fluoride onto mixed rare earth oxides. Sep Purif Technol 24:121–127. https://doi.org/10.1016/S1383-5866(00)00219-7

Rongshu W, Haiming L, Ping N, Ying W (1995) Study of a new adsorbent for fluoride removal from waters. Water Qual Res J Can 30:81–88. https://doi.org/10.2166/wqrj.1995.012

Saha I, Gupta K, Chakraborty S et al (2014) Synthesis, characterization and As(III) adsorption behavior of β-cyclodextrin modified hydrous ferric oxide. J Ind Eng Chem 20:1741–1751. https://doi.org/10.1016/j.jiec.2013.08.026

Saha I, Ghosh A, Nandi D et al (2015) β-Cyclodextrin modified hydrous zirconium oxide: Synthesis, characterization and defluoridation performance from aqueous solution. Chem Eng J 263:220–230. https://doi.org/10.1016/j.cej.2014.11.039

Saha I, Kanrar S, Gupta K et al (2016) Tuned synthesis and characterizational insight into β-cyclodextrin amended hydrous iron-zirconium hybrid oxide: a promising scavenger of fluoride in aqueous solution. RSC Adv 6:93842–93854. https://doi.org/10.1039/C6RA16567B

Sanchooli Moghaddam M, Rahdar S, Taghavi M (2016) Cadmium removal from aqueous solutions using saxaul tree ash. Iran J Chem Chem Eng 35:8

Siddiqui AH (1955) Fluorosis in Nalgonda District, Hyderabad-Deccan. Br Med J 2:1408–1413

Sivasamy A, Singh KP, Mohan D, Maruthamuthu M (2001) Studies on defluoridation of water by coal-based sorbents. J Chem Technol Biotechnol 76:717–722. https://doi.org/10.1002/jctb.440

Smedley PL, Kinniburgh DG (2002) A review of the source, behaviour and distribution of arsenic in natural waters. Appl Geochem 17:517–568. https://doi.org/10.1016/S0883-2927(02)00018-5

Taghavi M, Ehrampoush MH, Ghaneian MT et al (2018a) Application of a Keggin-type heteropoly acid on supporting nanoparticles in photocatalytic degradation of organic pollutants in aqueous solutions. J Clean Prod 197:1447–1453. https://doi.org/10.1016/j.jclepro.2018.06.280

Taghavi M, Ghaneian TM, Ehrampoush HM, Tabatabaee M, Afsharnia M, Alami A, J M (2018b) Feasibility of applying the LED-UV-induced TiO2/ZnO-supported H3PMo12O40 nanoparticles in photo catalytic degradation of aniline. Environ Monit Assess 190:188. https://doi.org/10.1007/s10661-018-6565-y

Tian Y, Wu M, Liu R et al (2011) Modified native cellulose fibers—a novel efficient adsorbent for both fluoride and arsenic. J Hazard Mater 185:93–100. https://doi.org/10.1016/j.jhazmat.2010.09.001

Viswanathan N, Sundaram CS, Meenakshi S (2009) Sorption behaviour of fluoride on carboxylated cross-linked chitosan beads. Colloids Surf B: Biointerfaces 68:48–54. https://doi.org/10.1016/j.colsurfb.2008.09.009

Wang B, Wu H, Yu L et al (2012) Template-free formation of uniform urchin-like α -FeOOH hollow spheres with superior capability for water treatment. Adv Mater 24:1111–1116. https://doi.org/10.1002/adma.201104599

Wang S, Gao B, Zimmerman AR et al (2015) Removal of arsenic by magnetic biochar prepared from pinewood and natural hematite. Bioresour Technol 175:391–395. https://doi.org/10.1016/j.biortech.2014.10.104

World Health Organization (ed) (2011) Guidelines for drinking-water quality, 4th edn. World Health Organization, Geneva

Yang X, Wang X, Feng Y et al (2013) Removal of multifold heavy metal contaminations in drinking water by porous magnetic Fe $_2$ O $_3$ @AlO(OH) superstructure. J Mater Chem A 1:473–477. https://doi.org/10.1039/C2TA00594H

Yang J, Zhang H, Yu M et al (2014) High-content, well-dispersed γ-Fe $_2$ O $_3$ nanoparticles encapsulated in macroporous silica with superior arsenic removal performance. Adv Funct Mater 24:1354–1363. https://doi.org/10.1002/adfm.201302561

Yavuz CT, Mayo JT, Yu WW et al (2006) Low-field magnetic separation of monodisperse Fe3O4 nanocrystals. Science 314:964–967. https://doi.org/10.1126/science.1131475

Yu X-Y, Xu R-X, Gao C et al (2012) Novel 3D hierarchical cotton-candy-like CuO: surfactant-free solvothermal synthesis and application in As(III) removal. ACS Appl Mater Interfaces 4:1954–1962. https://doi.org/10.1021/am201663d

Zhong L-S, Hu J-S, Liang H-P et al (2006) Self-assembled 3D flowerlike iron oxide nanostructures and their application in water treatment. Adv Mater 18:2426–2431. https://doi.org/10.1002/adma.200600504

Zhong L-S, Hu J-S, Wan L-J, Song W-G (2008) Facile synthesis of nanoporous anatase spheres and their environmental applications. Chem Commun:1184. https://doi.org/10.1039/b718300c